Precision & Performance Conference 2025, Cranfield University, UK, 17th- 20th November 2025

Development and validation of a simplified coil model for CFD simulation of a nano-positioning planar drive system

Ina Naujokat[1], Ludwig Herzog[1], Steffen Hesse[1], Parastoo Salimitari[1]
[1] *IMMS Institut für Mikroelektronik- und Mechatronik-Systeme gemeinnützige GmbH (IMMS GmbH)*

ina.naujokat@imms.de

Abstract
Rapidly developing demands on dynamics in nano-positioning systems lead to increased necessity of control systems to ensure accurate positioning capabilities. Direct driven structures use temperature control to minimize negative impact on positioning accuracy by thermal stress. Optimization of mentioned systems is realized by thermo- and fluid dynamic simulations.
This work shows a simplification approach of the geometrically complex structure of electrical coils for the CFD simulation of coil assemblies used for nano-positioning systems. By gathering information about coil structure and additional components like filling substances, a substitute material for the coil considering the influence of anisotropic material data such as thermal conductivity is generated and experimentally validated.

Numerical simulation, CFD, heat transfer, nano-positioning systems, model reduction

1. Introduction

Nano-positioning and nano-measurement techniques have great importance in various fields such as manufacturing and inspecting wafers, microelectronics and optics [1-4]. Recent advances have enabled the development of positioning systems with up to six degrees of freedom (6DOF) in closed loop control and sub-10 nm accuracy, for instance the NPS6D200 realized by IMMS GmbH in Ilmenau. This positioning system provides multiaxial motion by using a combination of lifting units and a planar drive system. The lifting units shown in Figure 1 as “LAU with planar guiding” positioned at the corners of the slider, allow the slider not only to be lifted in the vertical direction, but also to be tilted around the axes. To minimize friction between the moving slider and the stationary granite base, the slider is supported by air bearings. More detailed information on the system can be found in [4].

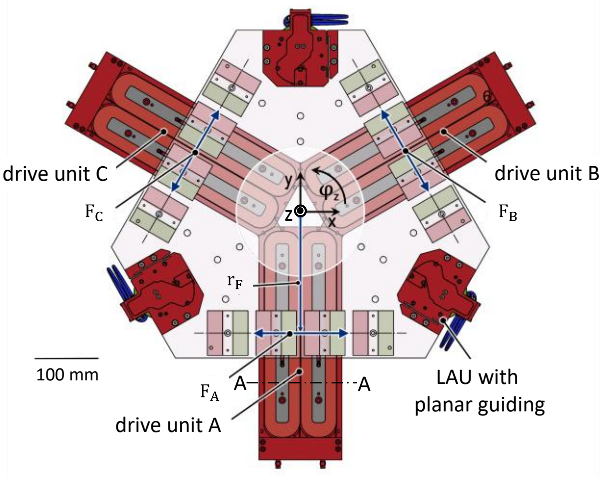

Figure 1: *Drive systems of the NPS6D200 [4]*

The horizontal positioning is realized by a linear drive system that enables the system to have a 200 mm positioning diameter. It consists of three stationary coil assemblies and corresponding permanent magnets attached to the moving slider. Based on the Lorentz force principle, the actuators create the positioning force.

The stationary components of the planar drive actuators include the so-called “coil assemblies”. The cross section A-A of “drive unit A” in Figure 1 is shown in Figure 2. Each coil assembly consists of two coils (4, 5) embedded in a cooling system. Inside the “cooling element sandwiches” (1) on top and on the bottom of the coils there is a thin cooling channel (3). The thin design of the channels minimizes the air gap, thereby increasing the motor constant and enhancing the resulting magnetic force.

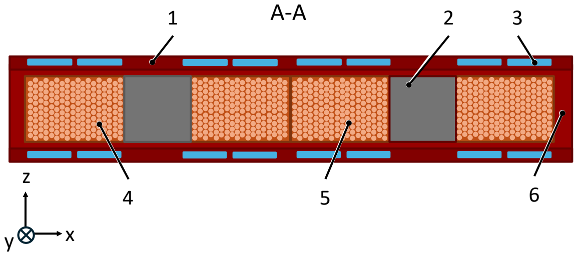

Figure 2: *Cross section of a coil assembly; 1 - cooling element sandwich (KKS), 2 - coil core, 3 - cooling channel, 4 - coil A1, 5 - coil A2, 6 - coil frame*

To optimize the thermal management of the coils, a simulation model is necessary. Simulations can be used for optimizing systems and identifying ineffective approaches and critical areas without requiring measurement equipment, invasive procedures or risking damage to the system.

Accurate simulation requires a thorough understanding of the coil’s structure. The coil consists of copper wires and various additional materials such as the filling material that ensure the functionality of the structure. To reduce the complexity of the 3D CAD model and therefore the computational expenses of CFD simulations, a simplified model is aspired that accurately represents the real coil [5].

This work presents the process of creating and simplifying a 3D CFD coil model, beginning with collecting more information about the coil's composition by metallographic analysis. Based on this analysis, the data for the simplified material is identified by reducing the detailed model and extracting the necessary data. Finally, the simplified model is validated experimentally.

2. Methodology

The overall goal of simulating the entire coil assembly including the cooling liquid leads to usage of ANSYS Fluent for coil simulation. By utilizing conjugated heat transfer (CHT), temperature gradients in solids are simulated efficiently.

In preparation for the microscopic analysis, the coil was divided into different sections and polished to account for the influence of the winding position on the composition.

Temperature measurements were conducted with thin film NTC thermistors. Each sensor was calibrated individually, and a fit function was generated from the calibration data to convert measured resistances into temperature values.

The deviation between experimental and simulated temperature data in contrast to the calculated measurement uncertainty serves as the key parameter for validation.

3. Microscopic analysis

To enhance understanding of how coil composition influences its thermal properties, sections of the coil were sanded and polished for microscopic evaluation of the materials and the winding pattern. As illustrated in Figure 3, the coils consist of copper wires (1), the insulation and baking varnish (2), a polyamide foil (3) that insulates the coil core from the wires, air cavities (4), the coil core and a filling material (6). Throughout the different sections around the coil, the exact winding structure as well as material composition varies.

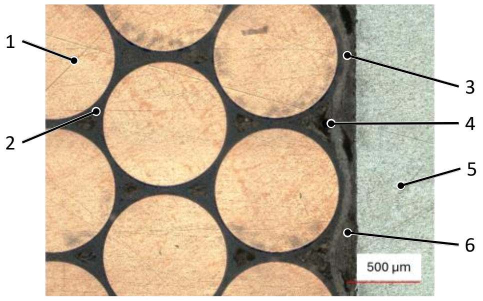

Figure 3: *Microscopic image of the coil; 1 - wire (copper), 2 - varnishes, 3 - polyamide foil, 4 - cavity (air), 5 - coil core (aluminum), 6 - filling material (thermal epoxy)*

The copper filling factor was determined through binarization of microscopic images. For binarization, MATLAB's image processing toolbox was used, and the procedure is illustrated in Figure 4 which led to a measured average filling factor of ≈ 71 %.

Based on microscopic analysis, average material properties such as density and specific heat capacity were applied as input parameters for the simulations.

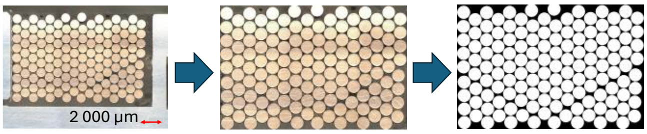

Figure 4: *Image processing for the binarization*

4. Numerical simulation

In addition to density and specific heat capacity, numerical heat transfer simulations require material specific thermal conductivities as input parameters. Due to wire curvature in the oval coil structure, as shown in Figure 1, the corresponding coordinate system defining heat transfer direction rotates simultaneously. To incorporate this, anisotropic material properties must be considered.

The following sections present the simulation procedures used for the determination of the thermal conductivities in the horizontal (*x*) and vertical (*z*) direction. In wire direction (*y*) no temperature gradient develops due to high thermal conductivity of the wires and definition of the coils as volumetric heat sources and therefore *y*-direction will not be considered separately. Additionally, simulations were conducted to quantify the deviation between the detailed and the reduced models. Furthermore, the influence of defining the reduced material as isotropic versus anisotropic is examined along with its impact on the model accuracy.

4.1. Thermal conductivity

The detailed geometry section used for simulating thermal conductivities as well as the associated mesh is shown in Figure 5. The model consists of 189 copper wires and a filling material derived from the additional materials identified in prior microscopic evaluations. To lower computational cost, the geometry was reduced in *y*-direction.

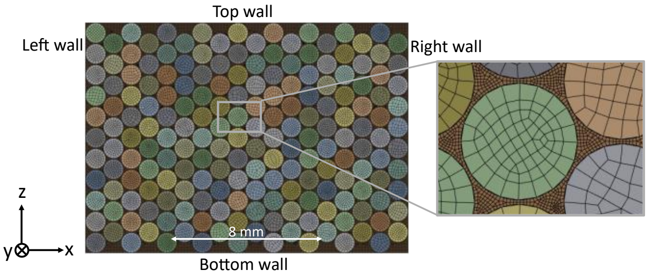

Figure 5: *Geometry and mesh for the estimation of the direction-dependent thermal conductivities*

The following boundary conditions were implemented at the illustrated walls:

Left wall: $\dot{q} = 50\,000 \frac{W}{m^2}$
Right wall: $T_c = 300\ K$
Top wall: Adiabatic
Bottom wall: Adiabatic

Based on the resulting temperature gradient (Figure 6) and the temperature at the left wall (T_H) the overall thermal conductivity in *x*-direction can be calculated by:

$$\lambda = \frac{\dot{q} \cdot d}{\Delta T} \qquad (1)$$

Where d is the distance between the left and right wall and $\Delta T = T_H - T_c$. The resulting temperature field shows the high thermal conductivity of copper with a homogeneous temperature distribution within the singular wires. The overall temperature gradient across the material shows a linear trend which leads to the assumption of a uniform thermal conductivity in *x*-direction for the simplified material.

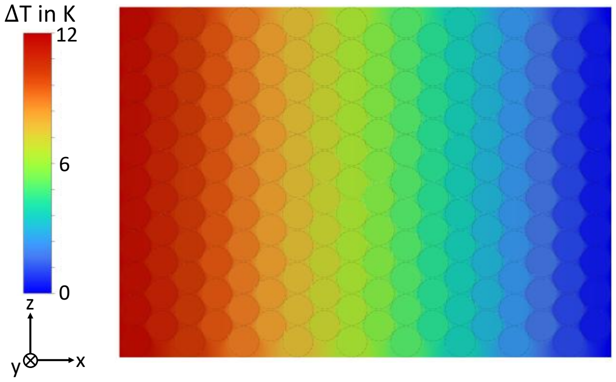

Figure 6: *Resulting temperature gradient of the simulation to determine the thermal conductivity in x-direction*

Similarly, thermal conductivity in the *z*-direction was determined by assigning a heat flux on the top wall and the temperature boundary condition on the bottom wall.

As a result, the thermal conductivities were calculated to be:

- $\lambda_x = 4\frac{W}{mK}$
- $\lambda_z = 3\frac{W}{mK}$

Since the wires are modeled as heat-generating volumes for the considered application and do not induce a temperature gradient along their length, it is not required to consider separate treatment of conductivity in the wire (*y*) direction.

4.2. Anisotropy of thermal conductivity

As shown in the previous section, thermal conductivity differs in the *x*- and *z*- directions for the analyzed geometry. To evaluate the influence of anisotropy, three separate simulations were conducted with equivalent boundary conditions.

Simulation one (S1) uses the same geometry and mesh setup as the earlier thermal conductivity simulations. Simulations two (S2) and three (S3) utilize a reduced geometry modeled as a homogeneous cuboid with equivalent external dimensions as S1. In S2, the previously calculated anisotropic thermal conductivities are applied while in S3, a surface-weighted average of the conductivities is used.

The input material data for simplified thermal simulations is summarized in Table 1:

Table 1: *Material data for the substitute material for thermal simulation of the coil*

Density	$\rho = 8000\ kg/m^3$
Thermal conductivity (*x, y*) for S2	$\lambda_{x,y} = 4\ W/(m\ K)$
Thermal conductivity (*z*) for S2	$\lambda_z = 3\ W/(m\ K)$
Average thermal conductivity for S3	$\lambda = 3.3\ W/(m\ K)$
Specific heat capacity	$c_p = 440\ J/(kg\ K)$

To generate and compare temperature gradients, a uniform volumetric heat source was applied to all three geometries. Figure 7 illustrates the resulting temperature fields from S1 (left) and S2 (right). The reduced model shows a higher overall temperature rise compared to the detailed model, predicating an overestimation of the thermal conductivity, although the shape of the temperature distribution remains similar. As the coil's thermal influence on its environment is of interest, comparison of resulting heat fluxes on the geometry walls is more eligible to quantify the accuracy of the simplified model.

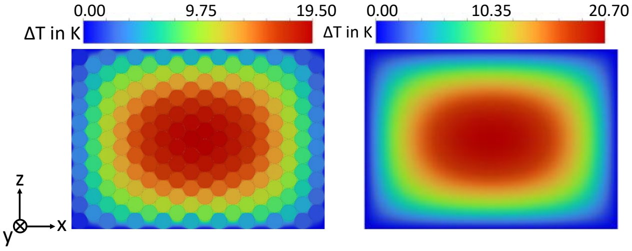

Figure 7: *Resulting temperature gradients for the detailed model (S1, left) and the simplified model with a direction-dependent thermal conductivity (S2, right)*

The results are presented in Table 2. As shown, the deviation between S2 - where directional thermal conductivity is applied - and S1 is negligible while a more significant deviation is observed between S3 and S1. This indicates that by considering anisotropic thermal conductivity, the generated reduced material model is eligible for reliable representation of the coil's thermal behavior in further simulations.

Table 2: *Resulting percentual heat flux deviations between the detailed model and the simulation with direction-dependent thermal conductivity (S2/S1) and deviation between the detailed model and the simulation with an average thermal conductivity (S3/S1)*

	Deviation S2 / S1 in %	Deviation S3 / S1 in %
Left wall	-3.40	-14.80
Right wall	-2.82	-14.29
Top wall	5.57	14.88
Bottom wall	5.56	14.88

5. Model validation

5.1 Experimental setup

Figure 8 depicts the experimental setup used for validating the simulation model. It shows the coil consisting of the coil windings (4) and the coil core (3), as well as the measurement equipment utilized and the electrical contacts (1). NTC thermistors (2) are attached by a heat-conducting paste to eliminate air gaps between the sensors and the wires. Copper foil is used to secure the sensors to the coil, to ensure a homogeneous temperature field around the sensitive area of the thermistor and to reduce the environmental influence on the measurements. Moreover, the experiments were executed in an insulated environment to resemble quasi-adiabatic boundary conditions. Consequently, the system did not reach a steady state, and thus the experiments were time-dependent.

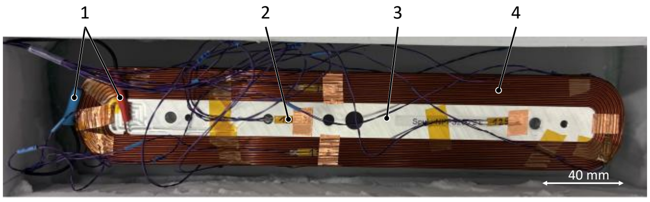

Figure 8: *Experimental setup to validate the simplified simulation of a coil; 1 - electrical contacts, 2 - temperature sensors, 3 - coil core, 4 - coil windings*

Measurements were taken at 30 s intervals over a duration of 300 s – 600 s depending on the operating power. To examine a wide range of applications, powers of 0.5 W, 1 W, 2 W, 5 W and 10 W were considered.

Finally, expanded measurement uncertainty was calculated to be $U_t = \pm 436\, mK$ with a safety factor of $k = 2$ to ensure accurate uncertainty estimation.

5.2 Simulation

To ensure accurate comparability between the experimental and simulation results, the boundary conditions for the simulations were derived from the experimental setup and summarized in Table 3:

Table 3: *Simulation boundary conditions*

Power	0.5 W, 1 W, 2 W, 5 W, 10 W
Outside walls	Adiabatic
Simulation time	300 s / 600 s
Time step size	1 s

A time-step size of one second was chosen to enable accurate temporal interpolation between exact measurement points.

Figure 9 shows the simulated temperature distribution across the coil surface for a power of P = 0.5 W on the coil, observed at time-steps 0 s, 300 s and 600 s. As illustrated, the temperature on the coil-winding surface and the coil-core surface does not rise at the same rate, indicating significant thermal contact resistance between these sections. By iteratively adapting the thermal contact definition, close agreement with the experimental results was archived, as discussed in the following section.

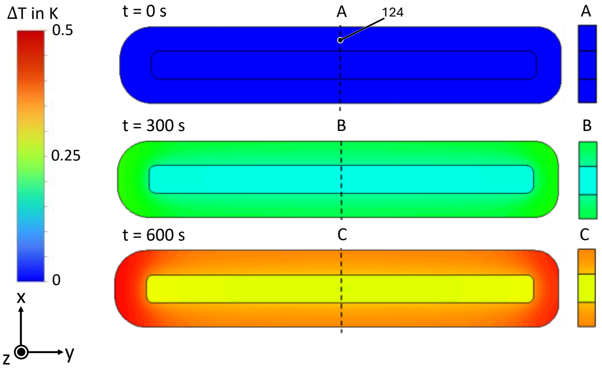

Figure 9: *Simulated temperature distribution on one coil with coil core for P = 0.5 W and a simulation time of 0 s, 300 s and 600 s*

5.3 Comparison of simulation and experimental results

Figure 10 displays sensor number 124 (see Figure 9) as a representative example, showing an average level of deviation compared to all measured points. It presents the rise in temperature on the coil surface from both experimental and simulation data for different power inputs. As illustrated, deviation rises with an increase in power. Quantification of divergence by comparing the absolute temperature values is collected in Table 4 showing the minimum, maximum and average deviations of all considered sensors as a function of power.

As depicted, deviation between simulation and experimental data is within measurement uncertainty. Thus, the reduced model resembles the real coil as a heat source within the validated range of power.

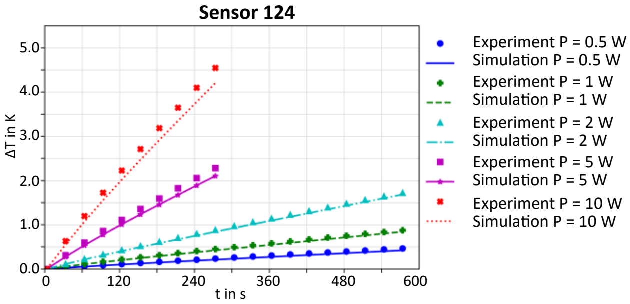

Figure 10: *Comparison of the temperature development of the coil between the simulation and the experiment exemplary for sensor 124*

Table 4*: Resulting deviations between the simulation and the experiment*

P in W	ΔT_{min} in mK	ΔT_{av} in mK	ΔT_{max} in mK
0.5	0.04	32	65
1	0.7	29	78
2	0.8	54	206
5	3	110	340
10	7	220	640

6. Conclusion

The results presented in this work demonstrate that the proposed procedure for reducing a complex, multi-material coil structure into a simplified material model is suitable for further thermal analyses. The reduced model accurately captures the coil's thermal behavior as a heat source within the validated power range, while significantly improving computational efficiency.

In addition, the methodology shows potential for broader application. Generalizing this reduction approach to accommodate various coil geometries — and extending it to simulations of entire coil assemblies in a nano-positioning system — represents a promising direction for future research.

Funding

The research group 'Application of AI-based virtual sensor technology to effectively increase the precision of positioning systems – VirtuSen' is funded by the German Land of Thüringen.

References

[1] Stauffenberg J, Reibe M, Krötschl A, Reuter C, Ortlepp I, Dontsov D, Hesse S, Rangelow I, Strehle S and Manske E 2023 Tip-based nanofabrication below 40 nm combined with a nanopositioning machine with a movement range of Ø 100 mm *Micr. and nano engin.* **19** 100201

[2] Chen Y, Zhiwen S, Zhang S, Zeng P, Liang H, Zheng M and Duan H 2021 Sub-10 nm fabrication: methods and applications *Int. J. Extrem. Manuf.* **3** 032002

[3] Huang W, Wang X, Meng Y, Li L, Zhang X, Ren M and Zhu L 2024 Design, modeling and control of high-bandwidth nano-positioning stages for ultra-precise measurement and manufacturing: a survey *Int. J. Exterm. Manuf.* **6**062007

[4] Hesse S, Huaman A, Katzschmann M, Leistritz B and Herzog L 2024 NPS6D200-A Long Range Nanopositioning Stage with 6D Closed Loop Control *Appl. Sci.* **14** 6972

[5] Chan W, D'Ambrogio A, Zacharewicz G, Mustafee N, Wainer G and Page E 2017 Approaches for simulation model simplification *Proc. 2017 Wint. Sim. Conf.* 4197-4208